Journal of Nuclear Medicine, published on January 18, 2018 as doi:10.2967/jnumed.117.203109

Head-to-head comparison of ^{11}C-PBR28 and ^{18}F-GE180 for the quantification of TSPO in the human brain

Paolo Zanotti-Fregonara[1], Belen Pascual[1], Gaia Rizzo[2,3], Meixiang Yu[1], Neha Pal[1], David Beers[1], Randall Carter[4], Stanley H. Appel[1], Nazem Atassi[5], Joseph C. Masdeu[1].

1 Nantz National Alzheimer Center and Houston Methodist Neurological Institute, and Weill Cornell Medicine, Houston, Texas
2 Invicro, London, UK
3 Division of Brain Sciences, Department of Medicine, Imperial College London, London, UK
4 GE Global Research, Schenectady, New York
5 Neurological Clinical Research Institute, Massachusetts General Hospital, Boston, Massachusetts

Word count: 6443

Running title: ^{18}F-GE180 vs. ^{11}C-PBR28

Corresponding author:

Paolo Zanotti Fregonara
Houston Methodist Research Institute
6670 Bertner St,
Houston, Texas 77030
Tel: 713-441-0803
Email: pzanottifregonara@houstonmethodist.org

Abstract

Introduction: ^{18}F-GE180 is a third-generation positron emission tomography (PET) tracer to quantify the translocator protein TSPO, a biomarker for inflammation. The aim of this study was to compare head-to-head ^{18}F-GE180 to the well-established translocator protein (TSPO) tracer ^{11}C-PBR28, by scanning with either tracer during the same day in the same subjects.
Materials and methods: Five subjects underwent a 90-minute PET scan with ^{11}C-PBR28 in the morning and ^{18}F-GE180 in the afternoon. A metabolite-corrected arterial input function was obtained in each subject for both tracers, and the brain uptake was quantified with a two-tissue compartmental model.
Results: The rate of metabolism of ^{18}F-GE180 in arterial blood was slower than that of ^{11}C-PBR28 (the percentages of unmetabolized parent in plasma at 90 minutes were 74.9 ± 4.15% and 11.2 ± 1.90%, respectively). The plasma free fraction was similar for both tracers: 3.5% ± 1.1 for ^{18}F-GE180 and 4.1% ± 1.1 for ^{11}C-PBR28. The average total volume of distribution (V_T) of ^{18}F-GE180 was about 20 times smaller than that of ^{11}C-PBR28 (0.15 ± 0.03 mL/cm^3 for ^{18}F-GE180 and 3.27 ± 0.66 mL/cm^3 for ^{11}C-PBR28). ^{18}F-GE180 was characterized by a poor transfer from the vascular compartment to the brain (K_1 was about ten times smaller than that of ^{11}C-PBR28). Moreover, kinetic modeling was more difficult with ^{18}F-GE180, as its V_T values were identified with a lower precision than those of ^{11}C-PBR28 and outlying values were more frequent.
Conclusion: The V_T of ^{18}F-GE180 is about 20 times smaller than that of ^{11}C-PBR28, due to a low penetration in the brain from the vascular compartment. In addition, kinetic modeling of ^{18}F-GE180 is more challenging than with ^{11}C-PBR28. Therefore, compared to ^{11}C-PBR28, ^{18}F-GE180 has unfavorable characteristics for TSPO imaging of the brain.

Introduction

The mitochondrial translocator protein 18 kDa (TSPO) is overexpressed in activated microglia in response to a variety of insults, such as tumors, physical injuries, strokes, as well as neurodegenerative and psychiatric conditions (*1-3*). Therefore, TSPO is commonly used as a biomarker to image and quantify glial activation with positron emission tomography (PET).

TSPO imaging with PET is however a challenging task, especially from a logistical point of view. TSPO is expressed in all brain regions and, except for well-defined clinical situations where a pseudo-reference region has been carefully validated for the disease under study (*4,5*), quantification requires serial blood sampling from an artery (*6*). Another logistical problem is that subjects must have a genotype analysis before the scan, because a single-nucleotide polymorphism (rs6971) affects the affinity of TSPO radioligand for the receptor (*7*). This polymorphism identifies three separate groups of subjects: high-, mixed-, and low-affinity binders. Low-affinity binders, which are about 5-10% of the Caucasian population, generally do not bind TSPO radioligands with sufficient affinity to be amenable to imaging, and the affinity difference between the two other groups needs to be taken into account to increase the statistical power of the study (*8*).

Also, TSPO ligands do not all perform equally well. The prototypical TSPO radioligand, ^{11}C-(*R*)-PK11195, has high lipophilicity and low specific binding (*9*). In recent years, several new radioligands with higher binding potential have been synthesized (*10*). For instance, the binding potential of ^{11}C-DPA-713 in humans is about ten times higher than that of ^{11}C-(*R*)-PK11195 (*11*). The affinity in vitro of PBR28 for high-affinity binders is also about ten times the affinity of PK11195 (*12*), and this translates into better in vivo imaging characteristics for ^{11}C-PBR28 compared ^{11}C-(*R*)-PK11195 in rodents (*13*), monkeys, and humans (*9*).

Quantification with ligands of higher affinity has however brought about another challenge. As immunohistochemical studies have shown, the density of TSPO is higher at the vessel walls of the blood-brain barrier compared to the brain tissue (*14*). Because of this heterogeneous distribution, the signal from the endothelium is disproportionately increased compared to the signal in the tissue (*1*). In order to properly take into account the endothelial uptake, an additional trapping compartment has been added to the compartmental model (*15,16*).

In quest of new radioligands with better properties, a novel tricyclic indole series of TSPO ligands has been recently developed. The best compound of the series, ^{18}F-GE180, displayed high affinity, good brain uptake and high specific binding in a neuroinflammation model (*17*). This tracer has been further tested in preclinical models of inflammation and proved to be superior to ^{11}C-(*R*)-PK11195 (*18-20*). In humans, ^{18}F-GE180 was amenable to quantification with compartmental modeling and Logan graphical analysis, but showed an unexpectedly low brain uptake (*21,22*).

The aim of this study was to perform a head-to-head comparison between ^{18}F-GE180 and a well-established second-generation TSPO tracer, ^{11}C-PBR28, by scanning with either tracer during the same day in the same subjects.

Materials and methods

Radiosynthesis

^{18}F-GE180 was manufactured following published procedures (*17*) with slight modifications by using a GE FASTlab synthesizer unit under FDA approved DMF (#21995). Briefly, a ^{18}F-fluoride solution with K_{222} and potassium bicarbonate was dried under azeotropic condition, and the radiolabeling was performed at 100 ^{o}C for 6 minutes in an acetonitrile solution. The radiolabeled product was trapped on the C18 cartridges, and the impurities were removed by 20 mL of the 40% v/v ethanol, followed by 11.5 mL of 35% v/v ethanol solution. The radiolabeled product ^{18}F-GE180 in the SPE cartridges was then eluted into a formulation buffer vial by using 55% v/v ethanol. The diluted product was then collected through a 0.22 µm filter. Total synthesis time was around 44 minutes with a specific radioactivity of 250 ± 101 GBq/µMol (N=5) and a yield of 22.0 ± 11.8 GBq (N=5).

^{11}C-PBR28 was manufactured following published procedures (*23*) with a slight modification using GE Tracerlab FX-MEI and FX-M modules. Briefly, the ^{11}C-CH_3I from TracerLab FX-M passed through a silver triflate (mixed with carbopack) oven (395 ^{o}F) to make ^{11}C-methyltriflate. The phenolic precursor (around 1 mg dissolved in 200 µL acetonitrile) was labeled with the ^{11}C-methyltriflate in a reaction vessel under basic condition (sodium hydride, 1-1.3 µg) at 35 ^{o}C for 3 min. The crude product was purified with preparative high-performance liquid chromatography (HPLC) using a mobile phase of methanol: 26.3 mM aqueous ammonium formate (62:38, v/v) at a flow rate of 5.5 mL/min, and the correct fraction was collected into a reservoir which was pre-filled with 50mL water. Then the mixed solution passed through a light C18 cartridge where PBR28 was trapped, and eluted with 1 mL ethanol followed by 9 mL saline. The solution was then transferred to the final product vial through a sterile filter (Millex GV filter, 0.22 µm). The total synthesis time was about 45 min, with specific radioactivity of 414 ± 94 GBq/µMol (N=5) and yield of 4.1 ± 1.6 GBq (N=5).

Subjects

Five subjects (3 men and 2 women, age 50.6 ± 17.6 years) participated in the study. Four were healthy volunteers and one was a patient with amyotrophic lateral sclerosis. Four subjects were mixed-affinity binders for TSPO radioligands and one healthy control was a high-affinity binder. Healthy subjects were free of current medical and psychiatric disorders, as determined by physical examination, laboratory urine and blood tests (including blood count and serum chemistry), and electrocardiogram. The vital sign of each subject were recorded before tracer injection and after the completion of the scan. All subjects had signed a written consent form for the study, which had been approved by the local Institutional Review Board.

Brain Imaging

PET images were acquired with a Philips Gemini TF 64 scanner. Subjects were laid on the bed scanner, with the head firmly held by a thermoplastic pillow and mask. After a computed tomography scan of the head acquired for attenuation correction, the subjects were injected in the morning with 622 ± 122 MBq of ^{11}C-PBR28 and in the afternoon with 178 ± 16 MBq of ^{18}F-GE180, using an automated pump. The two injections were at least three hours apart to allow for ^{11}C decay and biological removal. For both tracers, a dynamic scan was started at the moment of injection and stopped 90 minutes later.

Each subject underwent T1-weighted structural magnetic resonance imaging (MRI) for PET image co-registration. MRI was performed using a 3-dimensional magnetization-prepared rapid gradient-echo pulse sequence with an echo time of 3.04 ms, repetition time of 7.648 ms, inversion time of 900 ms, and flip angle of 8° on a 3-T whole-body scanner (Discovery, GE Medical Systems) with a Nova 32-channel phased-array head coil. The frames of the PET dynamic scans were first realigned and then coregistered to the structural MRI. Using the AAL-merged atlas implemented in the Pneuro module of Pmod 3.8 (Zurich, Switzerland), 71 brain regions were defined for each subject and a time-activity curve was obtained for each region. The brain time-activity curves were converted into standard uptake values (SUV) by normalizing the activity concentration for the injected activity and body weight.

Measurement of the input functions

Arterial blood samples for the PET scans performed with each tracer were drawn manually from the same catheter. For ^{11}C-PBR28, 24 blood samples (whose volume ranged from 1.5 to 6 mL) were drawn, initially every 15 seconds, and then at 4, 5, 6, 8, 10, 15, 20, 30, 40, 50, 60, 75, and 90 minutes. Each sample was centrifuged to separate the plasma from the blood cells, and the plasma was analyzed by high-performance liquid chromatography to separate the concentration of the parent from that of the radiometabolites. Chromatography was performed on the sample acquired at 5 minutes, and then on all the samples acquired from 10 minutes to the end of the scan. For ^{18}F-GE180, 23-25 samples were drawn with a volume ranging from 1.5 to 3 mL. The sampling schedule was similar to that of ^{11}C-PBR28, and chromatography was performed on at least 6 plasma samples per subject.
The measured fractions of parent were fitted with an extended Hill function (*24*), expressed as:

$$y(t) = 1 - \frac{a+bt}{\left(\frac{c}{t}\right)^{d}+1} \quad (1)$$

The fraction of parent was then multiplied by the total plasma activity, to obtain the time-activity curves of the parent concentrations for both tracers. These curves were then fitted with a tri-exponential function after relative weighting. The radioactivity concentration in whole blood was used to correct the brain activity that is due to the vascular compartment.
Finally, the plasma free fraction (f_P) was measured in duplicate for both tracers by ultrafiltration (*25*) and normalized using a standard derived from donor plasma.

Kinetic modeling

For both tracers, the input functions were fitted to the brain time-activity curves using a two-tissue compartment model (2TCM). Brain data were weighted by assuming that the standard deviation of the data was proportional to the inverse square root of the counts in the whole grey matter. The delay between the arrival of the tracers in the brain and in the radial artery was taken into account by fitting the whole grey matter.
We evaluated three different variants of the 2TCM: a model that assumed that the cerebral blood volume constituted 5% of total brain volume (2TCM_fix), a model in which the blood volume V_B was estimated along with the other microparameters (2TCM_V_B), and a model with an additional irreversible compartment that takes into account the trapping in the vascular walls (2TCM-1K) (*16*). The models were compared statistically with the Akaike Information Criterion (*26*), according to which the model

with the smallest value is the one that provides the best fit. In addition, both tracers were also quantified using a Logan graphical analysis, with t* fixed at 30 minutes.

Results

Plasma input functions

^{11}C-PBR28 concentrations peaked in plasma about 1-1.5 minutes after injection with a SUV value of 18.0 ± 5.65, and then progressively decreased (the average SUV concentration at 60 minutes was 0.19 ± 0.02) (Fig. 1A). ^{18}F-GE180 peaked at about the same time, with a SUV concentration of 35.4 ± 5.03, and decreased to 2.81 ± 0.19 at 60 minutes (Fig. 1B). The metabolism rate was much faster for ^{11}C-PBR28 than for ^{18}F-GE180: at 60 minutes, the percentages of unmetabolized parent in plasma were 11.2 ± 1.90% and 74.9 ± 4.15%, respectively (Fig. 1C). Interestingly, while for ^{11}C-PBR28 the SUV of the whole blood was constantly higher than the SUV of the parent concentration in plasma, for ^{18}F-GE180 the opposite was true. The average parent/whole blood ratio from 10 minutes to the end of the scan was 0.30 ± 0.07 for ^{11}C-PBR28 and 1.25 ± 0.06 for ^{18}F-GE180. The plasma free fraction was similar for both tracers: 3.5% ± 1.1 for ^{18}F-GE180 (n=5) and 4.1% ± 1.1 for ^{11}C-PBR28 (n=4, because the measurement in one subject failed).

Brain uptake and kinetic modeling

Visually, the brain uptake in the ^{11}C-PBR28 scans was much higher than that of the ^{18}F-GE180 scans. The activity of the vascular structures and the skull was prominent even in the summed image of the ^{18}F-GE180 scans, while no vascular activity was visible in the ^{11}C-PBR28 scans. The time-activity curves of ^{11}C-PBR28 showed a good uptake in the brain, with an increasing phase that reached its peak at about 8 minutes after injection (the peak SUV value in the whole brain was 1.90 ± 0.26), followed by a wash-out phase whose SUV at 90 minutes was 1.00 ± 0.20. By contrast, the highest value recorded in the ^{18}F-GE180 time-activity curves occurred at about 1.5 minutes after injection (SUV = 0.74 ± 0.15) and was likely due to vascular activity. After the initial vascular peaks, the curves were almost flat until the end of the scan. The peak that seems to be related with brain uptake occurred at about 7 minutes and had a SUV value of 0.67 ± 0.14. The SUV value at the end of the scan was 0.50 ± 0.09.

2TCM_fix produced good fitting with ^{11}C-PBR28: the fitting converged in all regions of all subjects, and in only 7 regions (out of 355, 71 per subject) V_T was estimated with a standard error (SE) greater than 20%. With ^{18}F-GE180, however, the fit was often poor in the initial part of the curve. Out of 355 regions, 92 regions had either a SE for V_T greater than 20% or the model did not converge. Fitting problems in the early part of the curve were noted also by Feeney and colleagues (*21*), who used a fixed V_B value, but not by Fan and colleagues (*22*), who estimated V_B along with the other microparameters.
The fitting was then repeated by estimating V_B (2TCM_V_B): for ^{11}C-PBR28, 4 regions out of 355 had a SE>20%, and all regions converged, and for ^{18}F-GE180 98/355 regions had either a SE>20% or the model did not converge. While the Akaike score did not change for ^{11}C-PBR28 when V_B was estimated (average value 126.6 ± 20.1 with 2TCM_fix and 121.2 ± 22.6 with 2TCM_V_B), it improved for ^{18}F-GE180 (40.9 ± 21.6 with 2TCM_fix and -2.7 ± 24.7 with 2TCM_V_B). These results contrast with those described in the study of Feeney, where the results with variable V_B did not outperform those with fixed V_B (*21*). We also tested a 2TCM with vascular trapping (2TCM-1K) and estimated V_B (*16*), but we found that in these five

subjects the Akaike score was very similar to that of the simple 2TCM_V_B (121.2 ± 24.7 for ^{11}C-PBR28 and -0.74 ± 25.8 for ^{18}F-GE180).
We therefore chose to compare the two tracers with a standard 2TCM_V_B, using only the regions where SE was smaller than 20% and where the model converged. We averaged the parameters of all subjects, because the V_T values of the amyotrophic patient were similar to those of the healthy volunteers, and the V_T values of the high-affinity binder were close to those of the mixed-affinity binders. The average ^{11}C-PBR28 V_T value was 3.27 ± 0.66 mL/cm^3, whereas the corresponding value for ^{18}F-GE180 was more than 20 times smaller (0.15 ± 0.03 mL/cm^3) (Table 1). In addition, the V_T of ^{11}C-PBR28 was estimated with greater precision than the V_T of ^{18}F-GE180. The average of the standard errors (considering only those smaller than 20%) was 4.03 ± 2.32% for ^{11}C-PBR28 and 7.00 ± 4.10% for ^{18}F-GE180.
Regarding the other modeling parameters, the main difference between the two tracers was found with K_1, which was ten times smaller for ^{18}F-GE180 than for ^{11}C-PBR28 (0.0070 ± 0.0016 vs. 0.0943 ± 0.0165 mL/min) (Table 1).
A similarly large difference in V_T values between the two tracers was obtained by using a Logan plot: 3.29 ± 0.61 mL/cm^3 for ^{11}C-PBR28 and 0.17 ± 0.03 mL/cm^3 for ^{18}F-GE180 (Fig. 3). The correlation between the 2TCM_V_B and Logan-V_T values was similar with both tracers (R^2 was 0.939 for ^{11}C-PBR28 and 0.901 for ^{18}F-GE180), although the analysis was performed only with the regions whose V_T value was well estimated (i.e. 351 for ^{11}C-PBR28 and 257 for ^{18}F-GE180).

Discussion

This study showed that ^{18}F-GE180, a new TSPO tracer, has a very low brain uptake. After kinetic modeling, the V_T values of ^{18}F-GE180 were more than 20 times smaller than those of the widely used ^{11}C-PBR28. The low brain uptake was mostly due to a low penetration into the brain from the vascular compartment. Indeed, a high activity inside the vessels was visible throughout the scans and the K_1 values of ^{18}F-GE180 were only about one tenth of those of ^{11}C-PBR28.

Kinetic modeling was also more difficult with ^{18}F-GE180 than with ^{11}C-PBR28. First, while ^{11}C-PBR28 gave good results with both 2TCM_fix and 2TCM_V_B models, the fittings of ^{18}F-GE180 curves were sometimes of poor quality if V_B was set at a fixed value. Second, ^{11}C-PBR28 gave good fittings in almost all regions and all subjects, but about one third of the regions analyzed with ^{18}F-GE180 had to be excluded because of a high SE or because the model did not converge. Third, the V_T values were estimated with higher precision with ^{11}C-PBR28 compared to ^{18}F-GE180.

There are several possible reasons why a TSPO tracer may have a low uptake in the brain. First, low-affinity binders do not show an appreciable specific binding with most TSPO tracers, but all subjects of this study were genotyped for the TSPO polymorphism, and all were either high or mixed-affinity binders. Then, the specific binding is proportional to the density of receptors and the affinity to the target. Each patient underwent both scans on the same day (^{11}C-PBR28 in the morning and ^{18}F-GE180 in the afternoon). This was done not only to minimize invasiveness (only one arterial catheter was placed) but also to minimize intra-subject variability in TSPO expression. The same-day retest variability of TSPO, measured with ^{11}C-PBR28, is about 16% (range 5-25%) (*27*), which of course cannot explain the 20-fold reduction in V_T found between the ^{11}C-PBR28 scans in the morning and the ^{18}F-GE180 scans in the

afternoon. Moreover, in vitro studies have shown that ^{18}F-GE180 has a good affinity for TSPO (Ki = 0.87 nM) (*17*).

A low f_P would limit the amount of free tracer available for tissue exchange. Indeed, this hypothesis to explain the low uptake of ^{18}F-GE180 in the brain was put forward by Fan et al., who were unable to estimate f_P reliably (*22*). In vitro experiments estimated the f_P of ^{18}F-GE180 at about 2-3% (*22*), and our own in vivo measurements showed that the f_P is about 3-4% of the parent activity in plasma, comparable to that of ^{11}C-PBR28. However, even if the percentage of the f_P is similar for both ligands, a low brain uptake could have been caused by a low exposure of the brain to the ligand, which ultimately depends on the amount of tracer present in the plasma. We therefore calculated a variable we called effective exposure (*E*), which is defined as the area under the curve of the input function during the first 20 minutes, multiplied by the free fraction, i.e. $AUC_{20} \times f_P$ (*28*). Table 2 compares the *E* values of ^{11}C-PBR28 and ^{18}F-GE180 to those of five other radioligands from the literature. Even in case of high parent concentrations due to a slow metabolism, an extremely low free fraction may result in a low exposure. Likely, this was the reason why ^{11}C-LY2428703, an mGluR1 tracer with excellent imaging characteristics in rodents (*29*), turned out to be unsuitable for human imaging (*28*). A low *E* may be compensated for by a high density of receptors or a high affinity, as it's probably the case for the CB1 ligand ^{18}F-FMPEP (*30*). Due to its slow metabolism in plasma, the *E* of ^{18}F-GE180 was much higher than that of ^{11}C-PBR28 (5.9 vs. 1.7), and more similar to that of the tracers ^{11}C-NOP1A and ^{11}C-(*R*)-rolipram (Table 2), which have a good brain uptake (*31, 32*). In summary, compared to ^{11}C-PBR28, ^{18}F-GE180 has a 20-fold lower brain uptake despite a more than 3-fold higher effective exposure.

Finally, a low brain uptake can be due to a low penetration of the blood brain barrier. Given that the Log$D_{7.4}$ of ^{18}F-GE180 is 2.95 (*21*), which is in the optimal range for passive brain entry in vivo (*33*), a low penetration due to a low lipophilicity is unlikely. ^{18}F-GE180 might however be a substrate for the efflux proteins at the blood brain barrier, such a P-glycoprotein. While this is probably the most plausible hypothesis, it should be noted that the parent/whole blood ratio of the input function of ^{18}F-GE180 was always higher than 1, which suggests that ^{18}F-GE180 cannot penetrate well into red cells either. The integrity of the blood brain barrier seems nevertheless necessary to prevent ^{18}F-GE180 from entering the brain. For instance, Albert and colleagues studied ^{18}F-GE180 uptake in patients with grade III or IV glioma and found an extraordinarily high tumor-to-background contrast (*34*). Such a high uptake, in our opinion, is mainly driven by the destruction of the blood brain barrier by the tumoral lesions. Albert and colleagues, however, suggested that the accumulation of ^{18}F-GE180 in the lesions is independent of the integrity of the blood brain barrier, especially because some peripheral areas of the lesions displayed ^{18}F-GE180 uptake without MR contrast enhancement. While it is more plausible that the contribution of TSPO expression to the overall uptake is higher in these peripheral areas, histological validation was not performed and, as the authors correctly state, it is known that the actual tumor volume exceeds the contrast-enhancement on MRI (*34-36*). Indeed, the brain tumor area defined by various PET tracers is commonly larger than that defined by MRI (*37-39*). It should be noted that small groups of glioma cells or even single invading cells are sufficient to cause a local breach of the blood brain barrier, even far away from the main tumor mass (*40*). Given the known limitations of MRI to depict areas with subtle permeability changes (*41,42*), the ^{18}F-GE180-positive/MRI-negative areas at the periphery of the glioma lesions may well be due to a more limited loss of integrity of the blood brain barrier, which would be visible thanks to the very low uptake of ^{18}F-GE180 in the normal areas of the brain.

Three previous studies tested ^{18}F-GE180 in humans, two in healthy volunteers (*21,22*) and one in glioma patients (*34*), and all of them recommended further evaluation of this tracer in patients with different inflammatory conditions. On the basis of our data, it is our contention that ^{18}F-GE180 is obviously inferior to the well-established ^{11}C-PBR28 for the study of brain inflammation, independently of blood-brain-barrier breakdown.

It is worth noting that a differential binding level between mixed and high-affinity binders was found by Fan and colleagues (*22*), but not by the other two studies who had a comparable number of subjects (*21,34*), and this despite a binding affinity in vitro of 15:1 between high and low-affinity binders (*21*). The lack of discrimination in vivo between genotype subgroups is likely due to the low brain uptake and the uncertainties in the quantification of noisy and almost flat brain time-activity curves with important vascular contaminations. If ^{18}F-GE180 cannot reliably detect known differences in binding affinity, then it should not be trusted to assess unknown differences in TSPO expression in patients with inflammatory conditions. Notably, new TSPO tracers whose imaging properties are better even than those of ^{11}C-PBR28 are now available. For instance, ^{11}C-ER176, a new quinazoline analog of ^{11}C-(*R*)-PK11195 (*43*), is characterized by a specific binding so high that even low-affinity binders can be successfully imaged (*44*).

The only advantage of ^{18}F-GE180 over ^{11}C-PBR28 is that the labeling with ^{18}F would allow using the tracer even in centers without a cyclotron. However, other ^{18}F-labeled TSPO radioligands with better properties are already available. For instance, ^{18}F-PBR06 is similar in terms of precision, sensitivity to accumulation of radiometabolites and magnitude of in vivo binding to its carbonated analog ^{11}C-PBR28 (*45*). Of course, using ^{18}F instead of ^{11}C would also deliver a higher radiation dose to the patient. Although the dosimetry of ^{18}F-GE180 has never been reported, the dose delivered by ^{18}F-tracers is about four times higher than that delivered by ^{11}C-tracers (*46,47*). It's our contention, however, that within this range of doses dosimetry should not be a concern, and the choice of the tracer should only be driven by imaging quality.

Finally, although poorly suited for human imaging, ^{18}F-GE180 has good imaging characteristics for preclinical models. Not only it is superior to ^{11}C-(*R*)-PK11195 in rodents (*18-20*), but also enables detection of microglial activation in a mouse model of Alzheimer's disease with greater sensitivity than ^{18}F-PBR06 (*48*). This suggests that ^{18}F-GE180 might be a substrate for efflux proteins at the blood-brain barrier in humans, but not in rodents (assuming that the blood-brain barrier is the reason for the poor uptake in humans). Species differences in permeability are not uncommon. More often, substances that are blocked by the rodents' barrier are taken up by the human brain, but the opposite also happens (*49*). Besides preclinical imaging, ^{18}F-GE180 might be useful also to image inflammation where there is no blood-brain barrier to cross (e.g. cardiovascular or peripheral oncologic diseases).

Conclusion

The V_T of ^{18}F-GE180 is about 20 times smaller than that of ^{11}C-PBR28, due to a low penetration in the brain from the vascular compartment. In addition, kinetic modeling of ^{18}F-GE180 is more challenging than with ^{11}C-PBR28, as its parameters are identified with a lower precision and outlying values are

more frequent. Therefore, compared to existing radioligands, ^{18}F-GE180 has unfavorable characteristics for TSPO imaging in the human brain.

Disclosure

Carter Randall is a GE employee. Joseph Masdeu is on a General Electric Healthcare advisory board and receives research support from GE, Eli Lilly, Biogen, Abbvie and Novartis.
The other authors declare that there is no conflict of interest.
This study was partially funded by ALS Finding a Cure and ALS Association, as part of the TRACK ALS protocol and the Harrison, Chao, Graham, and Nantz Funds of the Houston Methodist Foundation.

References

1. Turkheimer FE, Rizzo G, Bloomfield PS, et al. The methodology of TSPO imaging with positron emission tomography. *Biochem Soc Trans.* 2015;43:586-592.

2. Gershen LD, Zanotti-Fregonara P, Dustin IH, et al. Neuroinflammation in Temporal Lobe Epilepsy Measured Using Positron Emission Tomographic Imaging of Translocator Protein. *JAMA Neurol.* 2015;72:882-888.

3. Kreisl WC, Lyoo CH, McGwier M, et al. In vivo radioligand binding to translocator protein correlates with severity of Alzheimer's disease. *Brain.* 2013;136:2228-2238.

4. Lyoo CH, Ikawa M, Liow JS, et al. Cerebellum Can Serve As a Pseudo-Reference Region in Alzheimer Disease to Detect Neuroinflammation Measured with PET Radioligand Binding to Translocator Protein. *J Nucl Med.* 2015;56:701-706.

5. Albrecht DS, Normandin MD, Shcherbinin S, et al. Pseudo-reference regions for glial imaging with 11C-PBR28: investigation in two clinical cohorts. *J Nucl Med.* 2017. In press

6. Zanotti-Fregonara P, Chen K, Liow JS, Fujita M, Innis RB. Image-derived input function for brain PET studies: many challenges and few opportunities. *J Cereb Blood Flow Metab.* 2011;31:1986-1998.

7. Owen DR, Yeo AJ, Gunn RN, et al. An 18-kDa Translocator Protein (TSPO) polymorphism explains differences in binding affinity of the PET radioligand PBR28. *J Cereb Blood Flow Metab.* 2012;32:1-5.

8. Kreisl WC, Jenko KJ, Hines CS, et al. A genetic polymorphism for translocator protein 18 kDa affects both in vitro and in vivo radioligand binding in human brain to this putative biomarker of neuroinflammation. *J Cereb Blood Flow Metab.* 2013;33:53-58.

9. Kreisl WC, Fujita M, Fujimura Y, et al. Comparison of [(11)C]-(R)-PK 11195 and [(11)C]PBR28, two radioligands for translocator protein (18 kDa) in human and monkey: Implications for positron emission tomographic imaging of this inflammation biomarker. *Neuroimage.* 2010;49:2924-2932.

10. Herrera-Rivero M, Heneka M, Papadopoulos V. Translocator protein and new targets for neuroinflammation. *Clin and Transl Imaging.* 2015;3:391-402.

11. Kobayashi M, Jiang T, Telu S, et al. 11C-DPA-713 has much greater specific binding to translocator protein 18 kDa (TSPO) in human brain than 11C-(R)-PK11195. *J Cereb Blood Flow Metab.* 2017:271678x17699223.

12. Owen DR, Howell OW, Tang SP, et al. Two binding sites for [3H]PBR28 in human brain: implications for TSPO PET imaging of neuroinflammation. *J Cereb Blood Flow Metab.* 2010;30:1608-1618.

13. Parente A, Feltes PK, Vallez Garcia D, et al. Pharmacokinetic Analysis of 11C-PBR28 in the Rat Model of Herpes Encephalitis: Comparison with (R)-11C-PK11195. *J Nucl Med.* 2016;57:785-791.

14. Turkheimer FE, Edison P, Pavese N, et al. Reference and target region modeling of [11C]-(R)-PK11195 brain studies. *J Nucl Med.* 2007;48:158-167.

15. Wimberley C, Lavisse S, Brulon V, et al. Impact of endothelial TSPO on the quantification of 18F-DPA-714. *J Nucl Med.* 2017.

16. Rizzo G, Veronese M, Tonietto M, Zanotti-Fregonara P, Turkheimer FE, Bertoldo A. Kinetic modeling without accounting for the vascular component impairs the quantification of [(11)C]PBR28 brain PET data. *J Cereb Blood Flow Metab.* 2014;34:1060-1069.

17. Wadsworth H, Jones PA, Chau WF, et al. [(1)(8)F]GE-180: a novel fluorine-18 labelled PET tracer for imaging Translocator protein 18 kDa (TSPO). *Bioorg Med Chem Lett.* 2012;22:1308-1313.

18. Boutin H, Murray K, Pradillo J, et al. 18F-GE-180: a novel TSPO radiotracer compared to 11C-R-PK11195 in a preclinical model of stroke. *Eur J Nucl Med Mol Imaging.* 2015;42:503-511.

19. Dickens AM, Vainio S, Marjamaki P, et al. Detection of microglial activation in an acute model of neuroinflammation using PET and radiotracers 11C-(R)-PK11195 and 18F-GE-180. *J Nucl Med.* 2014;55:466-472.

20. Sridharan S, Lepelletier FX, Trigg W, et al. Comparative Evaluation of Three TSPO PET Radiotracers in a LPS-Induced Model of Mild Neuroinflammation in Rats. *Mol Imaging Biol.* 2017;19:77-89.

21. Feeney C, Scott G, Raffel J, et al. Kinetic analysis of the translocator protein positron emission tomography ligand [18F]GE-180 in the human brain. *Eur J Nucl Med Mol Imaging.* 2016;43:2201-2210.

22. Fan Z, Calsolaro V, Atkinson RA, et al. Flutriciclamide (18F-GE180) PET: First-in-Human PET Study of Novel Third-Generation In Vivo Marker of Human Translocator Protein. *J Nucl Med.* 2016;57:1753-1759.

23. Wang M, Yoder KK, Gao M, et al. Fully automated synthesis and initial PET evaluation of [11C]PBR28. *Bioorg Med Chem Lett.* 2009;19:5636-5639.

24. Tonietto M, Rizzo G, Veronese M, et al. Plasma radiometabolite correction in dynamic PET studies: Insights on the available modeling approaches. *J Cereb Blood Flow Metab.* 2016;36:326-339.

25. Gandelman MS, Baldwin RM, Zoghbi SS, Zea-Ponce Y, Innis RB. Evaluation of ultrafiltration for the free fraction determination of single photon emission computed tomography (SPECT) tracers: ß-CIT, IBF, and iomazenil. *J Pharm Sci.* 1994;83:1014-1019.

26. Akaike H. A new look at the statistical model identification. *IEEE Trans Automat Contr.* 1974;AC19:716-723.

27. Collste K, Forsberg A, Varrone A, et al. Test-retest reproducibility of [(11)C]PBR28 binding to TSPO in healthy control subjects. *Eur J Nucl Med Mol Imaging.* 2016;43:173-183.

28. Zanotti-Fregonara P, Barth VN, Zoghbi SS, et al. 11C-LY2428703, a positron emission tomographic radioligand for the metabotropic glutamate receptor 1, is unsuitable for imaging in monkey and human brains. *EJNMMI Res.* 2013;3:47.

29. Zanotti-Fregonara P, Barth VN, Liow JS, et al. Evaluation in vitro and in animals of a new 11C-labeled PET radioligand for metabotropic glutamate receptors 1 in brain. *Eur J Nucl Med Mol Imaging.* 2013;40:245-253.

30. Terry GE, Hirvonen J, Liow JS, et al. Imaging and quantitation of cannabinoid CB1 receptors in human and monkey brains using (18)F-labeled inverse agonist radioligands. *J Nucl Med.* 2010;51:112-120.

31. Zanotti-Fregonara P, Zoghbi SS, Liow JS, et al. Kinetic analysis in human brain of [11C](R)-rolipram, a positron emission tomographic radioligand to image phosphodiesterase 4: a retest study and use of an image-derived input function. *Neuroimage.* 2011;54:1903-1909.

32. Lohith TG, Zoghbi SS, Morse CL, et al. Brain and whole-body imaging of nociceptin/orphanin FQ peptide receptor in humans using the PET ligand 11C-NOP-1A. *J Nucl Med.* 2012;53:385-392.

33. Pike VW. PET radiotracers: crossing the blood-brain barrier and surviving metabolism. *Trends Pharmacol Sci.* 2009;30:431-440.

34. Albert NL, Unterrainer M, Fleischmann DF, et al. TSPO PET for glioma imaging using the novel ligand 18F-GE-180: first results in patients with glioblastoma. *Eur J Nucl Med Mol Imaging.* 2017.

35. Gilbert MR, Dignam JJ, Armstrong TS, et al. A randomized trial of bevacizumab for newly diagnosed glioblastoma. *N Engl J Med.* 2014;370:699-708.

36. Weller M, van den Bent M, Hopkins K, et al. EANO guideline for the diagnosis and treatment of anaplastic gliomas and glioblastoma. *Lancet Oncol.* 2014;15:e395-403.

37. Grosu AL, Weber WA, Riedel E, et al. L-(methyl-11C) methionine positron emission tomography for target delineation in resected high-grade gliomas before radiotherapy. *Int J Radiat Oncol Biol Phys.* 2005;63:64-74.

38. Zhao F, Li M, Wang Z, et al. (18)F-Fluorothymidine PET-CT for resected malignant gliomas before radiotherapy: tumor extent according to proliferative activity compared with MRI. *PLoS One.* 2015;10:e0118769.

39. Jacobs AH, Thomas A, Kracht LW, et al. 18F-fluoro-L-thymidine and 11C-methylmethionine as markers of increased transport and proliferation in brain tumors. *J Nucl Med.* 2005;46:1948-1958.

40. Watkins S, Robel S, Kimbrough IF, Robert SM, Ellis-Davies G, Sontheimer H. Disruption of astrocyte-vascular coupling and the blood-brain barrier by invading glioma cells. *Nat Commun.* 2014;5:4196.

41. Armitage PA, Farrall AJ, Carpenter TK, Doubal FN, Wardlaw JM. Use of dynamic contrast-enhanced MRI to measure subtle blood-brain barrier abnormalities. *Magn Reson Imaging.* 2011;29:305-314.

42. Cramer SP, Larsson HB. Accurate determination of blood-brain barrier permeability using dynamic contrast-enhanced T1-weighted MRI: a simulation and in vivo study on healthy subjects and multiple sclerosis patients. *J Cereb Blood Flow Metab.* 2014;34:1655-1665.

43. Zanotti-Fregonara P, Zhang Y, Jenko KJ, et al. Synthesis and evaluation of translocator 18 kDa protein (TSPO) positron emission tomography (PET) radioligands with low binding sensitivity to human single nucleotide polymorphism rs6971. *ACS Chem Neurosci.* 2014;5:963-971.

44. Ikawa M, Lohith TG, Shrestha S, et al. 11C-ER176, a Radioligand for 18-kDa Translocator Protein, Has Adequate Sensitivity to Robustly Image All Three Affinity Genotypes in Human Brain. *J Nucl Med.* 2017;58:320-325.

45. Dickstein LP, Zoghbi SS, Fujimura Y, et al. Comparison of F-18- and C-11-labeled aryloxyanilide analogs to measure translocator protein in human brain using positron emission tomography. *Eur J Nucl Med Mol Imaging.* 2011;38:352-357.

46. Zanotti-Fregonara P, Innis RB. Suggested pathway to assess radiation safety of 11C-labeled PET tracers for first-in-human studies. *Eur J Nucl Med Mol Imaging.* 2012;39:544-547.

47. Zanotti-Fregonara P, Lammertsma AA, Innis RB. Suggested pathway to assess radiation safety of (1)(8)F-labeled PET tracers for first-in-human studies. *Eur J Nucl Med Mol Imaging.* 2013;40:1781-1783.

48. James ML, Belichenko NP, Shuhendler AJ, et al. [18F]GE-180 PET Detects Reduced Microglia Activation After LM11A-31 Therapy in a Mouse Model of Alzheimer's Disease. *Theranostics.* 2017;7:1422-1436.

49. Deo AK, Theil FP, Nicolas JM. Confounding parameters in preclinical assessment of blood-brain barrier permeation: an overview with emphasis on species differences and effect of disease states. *Mol Pharm.* 2013;10:1581-1595.

50. Brown AK, Kimura Y, Zoghbi SS, et al. Metabotropic glutamate subtype 5 receptors are quantified in the human brain with a novel radioligand for PET. *J Nucl Med.* 2008;49:2042-2048.

Figure 1

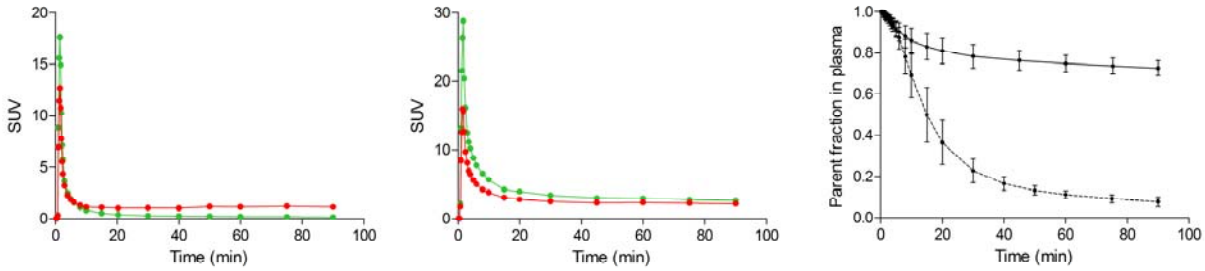

SUV concentrations of the parent compound (green lines) and the whole blood (red lines) for ^{11}C-PBR28 (A) and ^{18}F-GE180 (B) in a representative subject. While the parent concentration of ^{11}C-PBR28 is generally lower than the whole blood concentration, the opposite is true for ^{18}F-GE180. Panel C shows the average and standard deviation from all subjects of the parent fraction in plasma for ^{11}C-PBR28 (dashed line) and ^{18}F-GE180 (solid line). The metabolism rate is much slower for ^{18}F-GE180, as the parent constitutes about 70-80% of the total plasma activity at the end of the 90-minute scan.

Figure 2

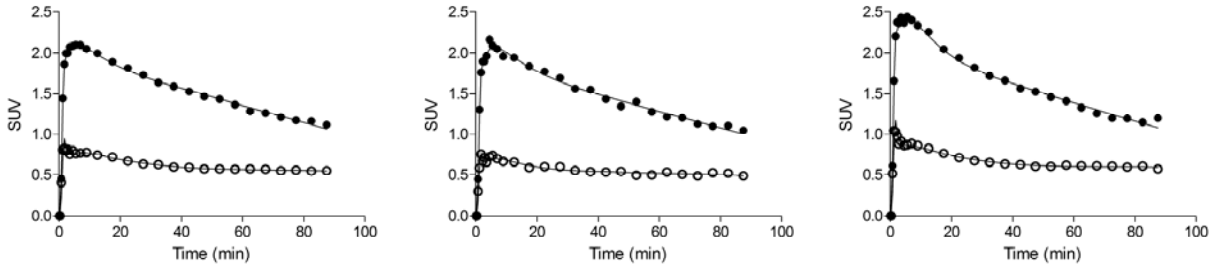

Time-activity curves, expressed in SUV, of three representative regions from the right hemisphere of the high-affinity binding healthy volunteer: (A) Temporal, (B) Putamen, and (C) Cerebellum. The SUV values of the ^{18}F-GE180 curves were substantially lower (peak value <1 SUV) than those of ^{11}C-PBR28 (peak value >2 SUV), and their shape was almost flat. The lines represent the fitting by a two-tissue compartment model.

Figure 3

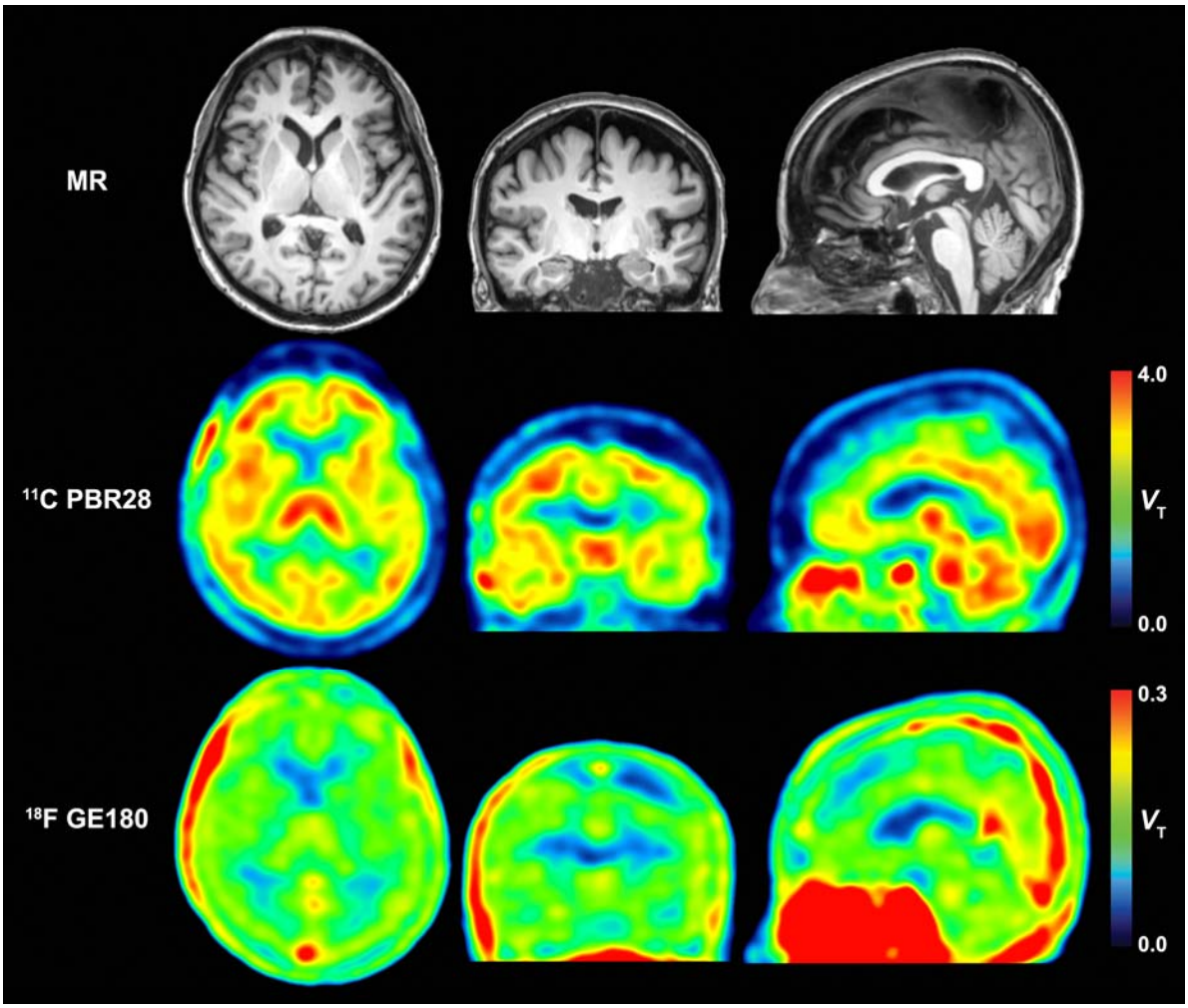

Parametric images of ^{11}C-PBR28 and ^{18}F-GE180, obtained with the Logan plot in the high-affinity binding healthy volunteer, shown along with the corresponding MR image for anatomical reference. ^{18}F-GE180 has a very low uptake in the brain, and by consequence the vascular structures are prominently visible.

Table 1: Comparison of kinetic modeling parameters of ^{11}C-PBR28 and ^{18}F-GE180 using a two-tissue compartment model

	K_1 (mL • cm^{-3} • min^{-1})		V_T (mL • cm^{-3})	
Region	*^{11}C-PBR28*	*^{18}F-GE180*	*^{11}C-PBR28*	*^{18}F-GE180*
Superior Frontal Cortex	0.090 ± 0.012 (2.0%)	0.0066 ± 0.0006 (5.4%)	3.22 ± 0.69 (2.1%)	0.15 ± 0.03 (6.3%)
Temporal Cortex	0.096 ± 0.013 (2.3%)	0.0070 ± 0.0006 (5.6%)	3.21 ± 0.75 (2.1%)	0.15 ± 0.02 (3.4%)
Parietal Cortex	0.085 ± 0.012 (2.8%)	0.0082 ± 0.0023 (9.6%)	3.04 ± 0.70 (3.0%)	0.14 ± 0.04 (3.8%)
Cerebellum	0.115 ± 0.014 (1.8%)	0.0077 ± 0.0011 (11.7%)	3.30 ± 0.70 (2.2%)	0.16 ± 0.05 (10.7%)
Average	**0.094 ± 0.017 (3.5%)**	**0.0070 ± 0.0016 (14.7%)**	**3.27 ± 0.66 (4.0%)**	**0.15 ± 0.03 (7.0%)**

Representative brain regions from the right hemisphere. Values are mean ± SD. Average standard errors are listed in parentheses and are expressed as % of the variable itself.

Table 2: Brain exposure for ^{11}C-PBR28 and ^{18}F-GE180, compared to that of five other radioligands, adapted from (*28*)

	^{11}C-PBR28	**^{18}F-GE180**	^{11}C-LY2428703 (*28*)	^{18}F-FMPEP (*30*)	^{18}F-SP203 (*50*)	^{11}C-(*R*)-Rolipram (*31*)	^{11}C-NOP1A (*32*)
Target	**TSPO**	**TSPO**	mGluR1	CB1	mGluR5	PDE4	NOP
Brain peak SUV	**~2**	**~0.7**	~0.5	3-4	~6	2-2.5	5-7
Exposure SUV (0-20)	**41.1**	**169.8**	202.2	47.8	37.0	124.9	36.7
f_p %	**4.1**	**3.5**	0.094	0.63	5.2	6.4	10.1
Effective exposure (E* f_p)	**1.7**	**5.9**	0.19	0.30	1.9	8.0	3.7